

Algorithms for Mitigating the Effect of Uncertain Geomagnetic Disturbances in Electric Grids

Minseok Ryu*, Harsha Nagarajan[†], Russell Bent[†]

*Department of Industrial & Operations Engineering, University of Michigan, Ann Arbor,

[†]Theoretical Division (T-5), Los Alamos National Laboratory, NM, U.S.A. (Contact: harsha@lanl.gov)

Abstract—Geomagnetic disturbances (GMDs), a result of space weather, pose a severe risk to electric grids. When GMDs occur, they can cause geomagnetically-induced currents (GICs), which saturate transformers, induce hot-spot heating, and increase reactive power losses in the transmission grid. Furthermore, uncertainty in the magnitude and orientation of the geo-electric field, and insufficient historical data make the problem of mitigating the effects of uncertain GMDs challenging. In this paper, we propose a novel distributionally robust optimization (DRO) approach that models uncertain GMDs and mitigates the effects of GICs on electric grids. This is achieved via a set of mitigation actions (e.g., line switching, locating blocking devices, generator re-dispatch and load shedding), prior to the GMD event, such that the worst-case expectation of the system cost is minimized. To this end, we develop a column-and-constraint generation algorithm that solves a sequence of mixed-integer second-order conic programs to handle the underlying convex support set of the uncertain GMDs. Also, we present a monolithic exact reformulation of our DRO model when the underlying support set can be approximated by a polytope with *three* extreme points. Numerical experiments on ‘epri-21’ system show the efficacy of the proposed algorithms and the exact reformulation of our DRO model.

Index Terms—Algorithms, Distributionally robust optimization, Geomagnetic disturbances, Line switching.

I. INTRODUCTION

Geomagnetic disturbances (GMDs) are caused by solar storms. During these storms charged particles escape from the sun, travel to the earth, create a geomagnetically-induced current (GIC), and impact electric transmission grids. Detrimental impacts include current distortions (harmonics), saturation of transformers, induced hot-spot heating, and increased reactive power losses [1], [2], [3] (see Figure 1). In 1989, the Hydro-Quebec power system was shut down for 9 hours due to a rare, but high-impact GMD, which led to a net loss of \$13.2 million [4].

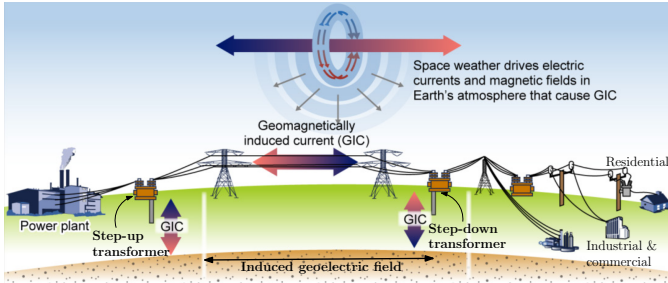


Fig. 1: Effect of GMDs on the electric grid. (Source: [1])

To mitigate the harmful effects of GMDs, one can install Direct Current (DC) blocking devices at regional substations to prevent the GICs, which is quasi-DC, from entering the power network through transformer neutrals [5]. This has led to work like [6] which posed the GIC blocking device placement problem that minimizes the costs of selecting appropriate locations to install these devices. Recently, numerous researchers have suggested that the risk of GICs could be reduced by the use of existing controls such as generator re-dispatch, line switching and load shedding. In [7], for the first time, the authors proposed an optimal transmission line switching (OTS) model under GMDs based on Alternating Current (AC) power flow equations and a set of constraints that captures GIC effects on various types of transformers. Utilizing state-of-the-art convex relaxations, the model was formulated as a mixed-integer quadratic convex program, which could be solved using commercial optimization solvers, albeit on small-scale instances. Recently, [8] presented heuristic-based algorithms to mitigate the effect of GICs on transformers by using line switching strategies on large-scale grids. Given that GMD events are hard to predict in advance and that the probability distribution of the uncertain magnitude and orientation of GMDs is not known precisely due to the insufficient historical data, [9] proposed a two-stage distributionally robust optimization (DRO) model with a mean-support ambiguity set and applied the standard column-and-constraint generation (CCG) algorithm [10] to solve on a small-scale instance, with prohibitively slow run times.

In this paper, we formulate a modified and an improved version of the two-stage DRO formulation presented in [9]. While [9] is focused on making the mitigation actions (line switching and generator dispatch) that hedges against the worst-case expected load shedding costs calculated based on the power flow equations at the second-stage, this paper focuses on making not only the mitigation actions but also their corresponding power flow operations at the first stage so as to minimize the worst-case expected damage costs due to GICs. This proposed decomposition also better represents the operation of electric grids from a practical perspective. Specifically, the first-stage problem models the AC Optimal Transmission Switching (AC-OTS) which determines active transmission lines and the set-points for generators which minimize the worst-case expected costs occurred by GMDs, i.e., taking expectation over the worst-case probability distribution among all the distributions in the ambiguity set. Given the solutions of the first-stage, the

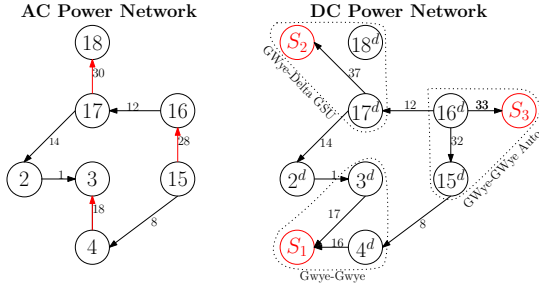


Fig. 2: An example of AC to DC network mapping

second-stage problem consists of linear constraints that capture the GIC effects. We assume the mean-support ambiguity set is provided and is uniform throughout the grid. The support set of the uncertain parameters is convex and can be approximated by a polytope with N extreme points. With these assumptions, the contributions of this paper are: (a) We first reformulate the two-stage DRO model as a min-max-min problem that can be solved by a CCG algorithm. [9] solves sub-problems which contain bilinear terms in the objective function, leading to weaker relaxations. To circumvent this issue, we solve a set of linear programs, each of which corresponds to an extreme point of the support set and enhances computation tractability. (b) For the special case of the support set with *three* extreme points ($N = 3$), we prove that the two-stage DRO model can be equivalently reformulated as a two-stage stochastic program with three scenarios. We further propose to construct a monolithic reformulation which can be solved efficiently using commercial solvers, and (c) We present a detailed numerical analysis on the ‘epri-21’ system, which is designed specifically for the GMD studies.

II. MATHEMATICAL FORMULATION

This section describes mathematical models that find a set of actions which mitigates the negative impacts of uncertain GMDs. Note that the formulation presented in this paper focuses on the quasi-static case (single time period) and leaves time-extended modeling for the future work.

A. AC and DC power network representation

The AC power network is represented by a graph $(\mathcal{N}, \mathcal{E})$, where \mathcal{N} is a set of nodes and \mathcal{E} is a set of arcs. This network is the standard representation used for modeling AC power flow physics in power system applications. The set \mathcal{E} is composed of \mathcal{E}^τ , a set of transformers, and $\mathcal{E} \setminus \mathcal{E}^\tau$, a set of transmission lines. The set \mathcal{N} is composed of buses that are adjacent to transmission lines and/or transformers. For calculating GICs (details in subsequent sections), which is a quasi-DC flow, we construct a DC power network $(\mathcal{N}^d, \mathcal{E}^d)$. \mathcal{N}^d includes buses in \mathcal{N} and additional nodes that model the neutral grounding points of transformers. The set \mathcal{E}^d includes transmission lines in \mathcal{E} and additional lines between the end points of transformers and their neutrals. The transformer configurations depend on the type of the transformer. In this paper, we consider 3 types of transformers, (i) Gwye-Gwye, (ii) GWye-GWye Auto, and (iii) GWye-Delta GSU. Detailed descriptions of these transformer types are found in [7], [9].

TABLE I: Nomenclature

Sets and parameters	
$\mathcal{G}, \mathcal{N}, \mathcal{E}$	a set of generators, buses, and lines in AC network
$\mathcal{E}^\tau \subseteq \mathcal{E}$	a set of transformers
$\mathcal{E}_i \subseteq \mathcal{E}$	a set of lines connected to $i \in \mathcal{N}$
c_k^{F0}	fixed cost when turning on $k \in \mathcal{G}$
c_k^{F1}, c_k^{F2}	fuel cost coefficients of power generation of $k \in \mathcal{G}$
g_k^r, g_k^i	bounds on the real power generation of $k \in \mathcal{G}$
g_k^r, g_k^i	bounds on the reactive power generation of $k \in \mathcal{G}$
κ_i	unit penalty cost for power unbalance at $i \in \mathcal{N}$
d_i^r, d_i^i	real and reactive power demand at $i \in \mathcal{N}$
u_i, v_i	voltage limits at $i \in \mathcal{N}$
g_e^s, b_e^s	shunt conductance and susceptance at $i \in \mathcal{N}$
g_e, b_e	conductance, susceptance of $e \in \mathcal{E}$
b_e^c	line charging susceptance of $e \in \mathcal{E}$
s_e	apparent power limit of line $e \in \mathcal{E}$
α_{ij}	tap ratio of $e_{ij} \in \mathcal{E}$
k_e	loss factor of transformer $e \in \mathcal{E}^\tau$
$\overline{l}_e^{\text{eff}}$	upper limit of the effective GICs on $e \in \mathcal{E}^\tau$
$\mathcal{N}^d, \mathcal{E}^d$	a set of nodes and arcs in DC network
$\mathcal{E}_m^d, \mathcal{E}_m^{d+}$	a set of incoming and outgoing arcs connected to $m \in \mathcal{N}^d$
γ_ℓ	conductance of $\ell \in \mathcal{E}^d$
a_m	inverse of ground resistance at $m \in \mathcal{N}^d$
\overline{v}^d	bound on the GIC-induced voltage magnitude
$\tilde{\xi}_\ell$	(random) GIC-induced voltage sources on $\ell \in \mathcal{E}^d$
Variables	
$z_e^a \in \mathbb{B}$	$z_e^a = 1$ if $e \in \mathcal{E}$ is turned on, and $z_e^a = 0$ otherwise
$z_k^g \in \mathbb{B}$	$z_k^g = 1$ if $k \in \mathcal{G}$ is turned on, and $z_k^g = 0$ otherwise
l_i^p, l_i^q	real power shedding at $i \in \mathcal{N}$
l_i^q, l_i^q	reactive power shedding at $i \in \mathcal{N}$
v_i	voltage magnitude at $i \in \mathcal{N}$
θ_i	phase angle at $i \in \mathcal{N}$
f_k^p, f_k^q	real and reactive power generated by $k \in \mathcal{G}$
p_{ei}, p_{ej}	real power flow on $e_{ij} \in \mathcal{E}$ from node i and to node j
q_{ei}, q_{ej}	reactive power flow on $e_{ij} \in \mathcal{E}$ from node i and to node j
w_i	$w_i = v_i^2, \forall i \in \mathcal{N}$
w_e^c	$w_e^c = v_i v_j \cos(\theta_i - \theta_j), \forall e_{ij} \in \mathcal{E}$
w_e^s	$w_e^s = v_i v_j \sin(\theta_i - \theta_j), \forall e_{ij} \in \mathcal{E}$
d_i^{loss}	allowable reactive power loss due to GICs at $i \in \mathcal{N}$
I_ℓ^d	GICs that flow on $\ell \in \mathcal{E}^d$
$\overline{l}_e^{\text{eff}}$	effective GICs on $e \in \mathcal{E}^\tau$
v_m^d	GIC-induced voltage magnitude at $m \in \mathcal{N}^d$

The mapping between the AC and DC network representations are described in Figure 2. In the AC network, $\mathcal{N} = \{2, 3, 4, 15, 16, 17, 18\}$, $\mathcal{E} = \{1, 8, 12, 14, 18, 28, 30\}$, and $\mathcal{E}^\tau = \{18, 28, 30\}$ (red arrows in Figure 2). The DC network $(\mathcal{N}^d, \mathcal{E}^d)$ is constructed by adding information on different types of transformers and their connection to neutral (red circles in Figure 2). We first add neutral nodes $\{S_1, S_2, S_3\}$, each of which is connected to a transformer. The set \mathcal{N} is relabeled with $\{2^d, 3^d, 4^d, 15^d, 16^d, 17^d, 18^d\}$ in the DC network. Topological mappings for different types of transformers are highlighted in Figure 2.

To link the two networks, we define functions E and E^{-1} that map $\ell \in \mathcal{E}^d$ to an edge $e \in \mathcal{E}$ and vice versa, i.e., if $E_\ell = e$, then $E_e^{-1} = \{\ell \in \mathcal{E}^d : E_\ell = e\}$. For example, line 17 in the DC network maps to the transformer line 18 in the AC network, thus $E_{17} = 18$. Transformer line 18 maps to lines 16 and 17 in DC network, thus $E_{18}^{-1} = \{16, 17\}$.

B. GIC calculation

This section describes the calculation of GICs and how they affect different types of transformers. Under the assumption

of an uniformly induced geo-electric field within an interconnected electric grid, GIC that flows on a line in the DC network is given by

$$I_\ell^d = \gamma_\ell(v_m^d - v_n^d + \tilde{\xi}_\ell), \forall \ell_{mn} \in \mathcal{E}^d$$

where, $\tilde{\xi}_\ell$ is the GIC-induced voltage source, given by:

$$\tilde{\xi}_\ell = \begin{cases} \tilde{\xi}_E L_\ell^E + \tilde{\xi}_N L_\ell^N, & \forall \ell \in \mathcal{E}^d : E_\ell \in \mathcal{E} \setminus \mathcal{E}^\tau, \\ 0, & \forall \ell \in \mathcal{E}^d : E_\ell \in \mathcal{E}^\tau \end{cases}$$

and $\tilde{\xi}_E$ and $\tilde{\xi}_N$ are *uncertain* geo-electric fields [V/km] in the eastward and northward direction, respectively, and L_ℓ^E and L_ℓ^N are the lengths [km] of transmission lines ℓ in the eastward and northward direction, respectively.

Based on the calculated GIC in the DC network, the effective GIC of a transformer in the AC network is given by

$$I_e^{\text{eff}} = |\Theta(I_\ell^d, \forall \ell \in E_e^{-1})|, \forall e \in \mathcal{E}^\tau$$

where $\Theta(I_\ell^d, \forall \ell \in E_e^{-1})$ is a linear function of GIC (I_ℓ^d). This function depends on the type of transformer as described in Table II. Note that (N_h, N_l, N_s, N_c) are parameters which indicate the number of turns in the high-side/low-side/series/common winding, respectively.

TABLE II: Effective GICs for each type of transformers

Type of transformer e	E_e^{-1}	$\Theta(I_\ell^d, \forall \ell \in E_e^{-1})$
Gweye-Gweye	$\{h, l\}$	$\Theta(I_h^d, I_l^d) = \frac{N_h I_h^d + N_l I_l^d}{N_h}$
GWye-GWye Auto	$\{s, c\}$	$\Theta(I_s^d, I_c^d) = \frac{N_s I_s^d + N_c I_c^d}{N_s + N_c}$
GWye-Delta GSU	$\{h\}$	$\Theta(I_h^d) = I_h^d$

Lastly, given \mathcal{E}_i^τ is a set of transformers connected to node i , the reactive power loss [6] due to GICs at node i in the AC network is calculated by

$$\sum_{e \in \mathcal{E}_i^\tau} k_e v_i I_e^{\text{eff}}, \forall i \in \mathcal{N} \quad (1)$$

C. Uncertainty set description

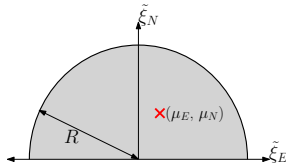


Fig. 3: Support set and mean of uncertain GMDs ($\tilde{\xi}_E, \tilde{\xi}_N$)

In this model, the geo-electric field ($\tilde{\xi}_E, \tilde{\xi}_N$) is uncertain when planning decisions are made to mitigate the risk of GMDs. We assume that the support set and mean values of ($\tilde{\xi}_E, \tilde{\xi}_N$) are provided or are extracted from a set of historical data, but their joint probability distribution is unknown. Generally, there is not enough information to construct reasonable probability distributions [11]. In this setting, we construct the following mean-support ambiguity set \mathcal{D} :

$$\mathcal{D} := \{\mathbb{P} : \mathbb{E}_{\mathbb{P}_E}[\tilde{\xi}_E] = \mu_E, \mathbb{E}_{\mathbb{P}_N}[\tilde{\xi}_N] = \mu_N, \mathbb{P}\{\tilde{\xi} \in \Xi\} = 1\}$$

where ($\mathbb{P}_E, \mathbb{P}_N$) and (μ_E, μ_N) are the marginal distributions and mean values of ($\tilde{\xi}_E, \tilde{\xi}_N$), respectively. The support set Ξ of $\tilde{\xi} = (\tilde{\xi}_E, \tilde{\xi}_N)$ is defined as

$$\Xi := \left\{ \tilde{\xi} = (\tilde{\xi}_E, \tilde{\xi}_N) \in \mathbb{R}^2 : -R \leq \tilde{\xi}_E \leq R, 0 \leq \tilde{\xi}_N \leq R, (\tilde{\xi}_E)^2 + (\tilde{\xi}_N)^2 \leq R^2 \right\}$$

where R is a radius of half-circle support set as shown in Figure 3. Practically speaking, the support set is bounded by an estimate of the worst-case magnitude of the storm. Since the square of the magnitude is equal to the sum of the squares of the northward and eastward field strength, a magnitude bound yields a half circle support set for ($\tilde{\xi}_E, \tilde{\xi}_N$) [11].

D. Two-stage DRO formulation

In this section we describe a two-stage DRO formulation which determines a set of mitigation actions which minimizes the cost of generation and a penalty for shedding loads and is robust to the worst-case probability distribution in the ambiguity set \mathcal{D} as defined in section II-C. To preserve computational tractability, we use the second-order conic relaxations of the rectangular form of the nonlinear, nonconvex AC power flow constraints and formulate the first-stage problem as an MISOCP:

$$\begin{aligned} \min \quad & \sum_{k \in \mathcal{G}} (c_k^{\text{F0}} z_k^g + c_k^{\text{F1}} f_k^p + c_k^{\text{F2}} (f_k^p)^2) + \sum_{i \in \mathcal{N}} \kappa^1 (l_i^{p+} + l_i^{p-} + l_i^{q+} + l_i^{q-}) \\ & + \sup_{\mathbb{P} \in \mathcal{D}} \mathbb{E}_{\mathbb{P}}[\mathcal{Q}(z^a, v, d^{\text{loss}}, \tilde{\xi})] \quad (2a) \\ \text{s.t.} \quad & \sum_{e \in \mathcal{E}_i} p_{ei} = \sum_{k \in \mathcal{G}_i} f_k^p - d_i^p + l_i^{p+} - l_i^{p-} - g_i^s w_i, \forall i \in \mathcal{N}, \quad (2b) \\ & \sum_{e \in \mathcal{E}_i} q_{ei} = \sum_{k \in \mathcal{G}_i} f_k^q - d_i^q + l_i^{q+} - l_i^{q-} + b_i^s w_i - d_i^{\text{loss}}, \forall i \in \mathcal{N}, \quad (2c) \\ & p_{ei}^2 + q_{ei}^2 \leq z_e^a (\bar{s}_e^2), \quad p_{ej}^2 + q_{ej}^2 \leq z_e^a (\bar{s}_e^2), \forall e_{ij} \in \mathcal{E}, \quad (2d) \\ & p_{ei} = \frac{1}{\alpha_{ij}^2} g_e w_{ei}^z - \frac{1}{\alpha_{ij}} (g_e w_e^z + b_e w_e^z), \forall e_{ij} \in \mathcal{E}, \quad (2e) \\ & p_{ej} = g_e w_{ej}^z - \frac{1}{\alpha_{ij}} (g_e w_e^z - b_e w_e^z), \forall e_{ij} \in \mathcal{E}, \quad (2f) \\ & q_{ei} = -\frac{1}{\alpha_{ij}^2} (b_e + \frac{b_e^c}{2}) w_{ei}^z + \frac{1}{\alpha_{ij}} (b_e w_e^z - g_e w_e^z), \forall e_{ij} \in \mathcal{E}, \quad (2g) \\ & q_{ej} = -(b_e + \frac{b_e^c}{2}) w_{ej}^z + \frac{1}{\alpha_{ij}} (b_e w_e^z + g_e w_e^z), \forall e_{ij} \in \mathcal{E}, \quad (2h) \\ & w_{ei}^z \in \langle z_e^a, w_i \rangle^{\text{MC}}, \quad w_{ej}^z \in \langle z_e^a, w_j \rangle^{\text{MC}}, \forall e_{ij} \in \mathcal{E}, \quad (2i) \\ & \underline{w}_e^z z_e^a \leq \underline{w}_e^z \leq \bar{w}_e^z z_e^a, \quad \underline{w}_e^s z_e^a \leq \underline{w}_e^s \leq \bar{w}_e^s z_e^a, \forall e \in \mathcal{E}, \quad (2j) \\ & (w_e^z)^2 + (w_e^s)^2 \leq \underline{w}_e^z w_{ei}^z, \forall e_{ij} \in \mathcal{E}, \quad (2k) \\ & \tan(\underline{\theta}_{ij}) w_e^z \leq w_{ei}^z \leq \tan(\bar{\theta}_{ij}) w_e^z, \forall e_{ij} \in \mathcal{E}, \quad (2l) \\ & (v_i)^2 \leq w_i \leq (\bar{v}_i + \underline{v}_i) v_i - \bar{v}_i \underline{v}_i, \forall i \in \mathcal{N}, \quad (2m) \\ & \sum_{e \in \mathcal{E}_k} z_e^a \geq z_k^g, \forall k \in \mathcal{G}, \quad (2n) \\ & \underline{v}_i \leq v_i \leq \bar{v}_i, \quad l_i^{p+}, l_i^{p-}, l_i^{q+}, l_i^{q-} \geq 0, \forall i \in \mathcal{N}, \quad (2o) \\ & \underline{g}_k^p z_k^g \leq f_k^p \leq \bar{g}_k^p z_k^g, \quad \underline{g}_k^q z_k^g \leq f_k^q \leq \bar{g}_k^q z_k^g, \forall k \in \mathcal{G}, \quad (2p) \\ & z_e^a \in \{0, 1\}, \forall e \in \mathcal{E}, \quad z_k^g \in \{0, 1\}, \forall k \in \mathcal{G}. \quad (2q) \end{aligned}$$

where, given the values of $\mathbf{z}^a, \mathbf{v}, \mathbf{d}^{\text{loss}}$ from the first-stage problem (2) and the realization of $\tilde{\xi}$, $\mathcal{Q}(\mathbf{z}^a, \mathbf{v}, \mathbf{d}^{\text{loss}}, \tilde{\xi})$ is the optimal value of the following second-stage problem which evaluates GICs in the DC network:

$$\min \sum_{i \in \mathcal{N}} \kappa^s s_i \quad (3a)$$

$$\text{s.t. } \frac{I_\ell^d}{\gamma_\ell} \leq (v_m^d - v_n^d + \tilde{\xi}_\ell) + M_\ell^-(1 - z_{E_\ell}^a), \quad \forall \ell_{mn} \in \mathcal{E}^d, \quad (3b)$$

$$\frac{I_\ell^d}{\gamma_\ell} \geq (v_m^d - v_n^d + \tilde{\xi}_\ell) - M_\ell^+(1 - z_{E_\ell}^a), \quad \forall \ell_{mn} \in \mathcal{E}^d, \quad (3c)$$

$$-z_{E_\ell}^a M_\ell^- \leq \frac{I_\ell^d}{\gamma_\ell} \leq z_{E_\ell}^a M_\ell^+, \quad \forall \ell_{mn} \in \mathcal{E}^d, \quad (3d)$$

$$\sum_{\ell \in \mathcal{E}_m^{d-}} I_\ell^d - \sum_{\ell \in \mathcal{E}_m^{d+}} I_\ell^d = a_m v_m^d, \quad \forall m \in \mathcal{N}^d, \quad (3e)$$

$$I_e^{\text{eff}} \geq \Theta(I_\ell^d, \forall \ell \in E_e^{-1}), \quad I_e^{\text{eff}} \geq -\Theta(I_\ell^d, \forall \ell \in E_e^{-1}), \quad (3f)$$

$$0 \leq I_e^{\text{eff}} \leq \bar{I}_e^{\text{eff}}, \quad \forall e \in \mathcal{E}^r, \quad s_i \geq 0, \quad \forall i \in \mathcal{N} \quad (3g)$$

$$u_{ei}^d \in \langle v_i, I_e^{\text{eff}} \rangle^{\text{MC}}, \quad d_i^{\text{loss}} \geq \sum_{e \in \mathcal{E}_i^r} k_e u_{ei}^d - s_i, \quad \forall i \in \mathcal{N}. \quad (3h)$$

Constraints (2b)–(2p) model the relaxed AC power flow equations. These constraints include mitigation actions such as transmission line switching and switching of generators. Note that generator switching in this formulation *does not* imply that we model economic unit commitment. Constraints (2b) and (2c) model real and reactive power balance constraints, including allowable GIC-induced reactive power loss (d_i^{loss}). Constraints (2d) ensure that the apparent power flow does not exceed its limit when the line is closed. Constraints (2e)–(2h) model Ohm's law. Constraints (2i)–(2m) model the MISOCP relaxation of the AC power flow equations using the formulations discussed in [12]. Notation $\langle x_i, x_j \rangle^{\text{MC}}$ models the standard McCormick relaxation of a bilinear term $x_i \cdot x_j$, which is very effective for ACOPF problems [12], [13], [14], [15], [16], and also for generic nonlinear programs with bilinear terms [17]. Constraints (2n) ensure that a generator is turned off when all the lines and transformers connected to that generator are off.

In the second-stage problem, constraints (3b)–(3d) calculate valid GICs in the DC network for lines that are switched on. Else, they are deactivated with the big-M coefficients, where $M_\ell^+ = \bar{v}^d + \tilde{\xi}_\ell$, $M_\ell^- = \bar{v}^d - \tilde{\xi}_\ell$. Constraints (3e) model nodal balance equation for GICs in the DC network. Note that, in (3e), $a_m = 0$ when m is not a grounded neutral node. Constraints (3f) and (3g) calculate the effective GICs for each type of transformer (see Table II), which in-turn is used to calculate the reactive power losses induced in the AC network, as shown in constraints (3h).

Interpretation of the two-stage DRO formulation Once the uncertain GMDs ($\tilde{\xi}$) are realized and the decisions in the AC network on line switching (\mathbf{z}^a), voltage magnitude (\mathbf{v}), and allowable reactive power losses \mathbf{d}^{loss} (interpreted as the amount of reactive power loss that will not cause excessive voltage drops. Exceeding this value would correspond to the cost of installing or using a device to counteract the reactive losses), the second-stage problem calculates the effective GICs and

the actual reactive power losses, given by $\sum_{e \in \mathcal{E}_i^r} k_e u_{ei}^d$. If the calculated reactive power losses in second-stage exceeds the allowable \mathbf{d}^{loss} from the first-stage, then appropriate mitigation actions are updated in the AC network to mitigate the negative effects on the transformers. Implicitly, this formulation assumes that reactive losses smaller than \mathbf{d}^{loss} will not cause voltage problems (i.e., a high voltage).

In summary, the proposed two-stage DRO formulation minimizes the power generation cost, penalty cost for shedding loads and the worst-case expected cost occurred by damaged transformers.

III. SOLUTION METHODOLOGIES

In this section, we describe several solution approaches to the two-stage DRO formulation. For ease of exposition, we rewrite the formulation using matrix notation as follows:

$$\min_{\mathbf{z} \in \mathcal{F}} \mathbf{q}^T \mathbf{z} + \sup_{\mathbb{P} \in \mathcal{D}} \mathbb{E}_{\mathbb{P}}[\mathcal{Q}(\mathbf{z}, \tilde{\xi})] \quad (4a)$$

where $\mathcal{Q}(\mathbf{z}, \tilde{\xi})$ is the optimal value of the following problem:

$$\mathcal{Q}(\mathbf{z}, \tilde{\xi}) = \min_{\mathbf{x} \in \mathcal{X}(\mathbf{z}, \tilde{\xi})} \mathbf{c}^T \mathbf{x}. \quad (4b)$$

Note that \mathbf{z} and \mathcal{F} are the solution vector and the feasible region, respectively, of the first-stage problem (2) and $\mathcal{X}(\mathbf{z}, \tilde{\xi}) = \{\mathbf{x} \in \mathbb{R}^n : \mathbf{A}\mathbf{x} + \mathbf{B}(\tilde{\xi})\mathbf{z} \geq \mathbf{d}\}$ is the feasible region of the second-stage problem.

Proposition III.1. Problem (4) is equivalent to the following min-max-min problem:

$$\min_{\mathbf{z} \in \mathcal{F}} \mathbf{q}^T \mathbf{z} + \mu_E \lambda_E + \mu_N \lambda_N + \left\{ \max_{\tilde{\xi} \in \Xi} \left(\min_{\mathbf{x} \in \mathcal{X}(\mathbf{z}, \tilde{\xi})} \mathbf{c}^T \mathbf{x} \right) - \lambda_E \tilde{\xi}_E - \lambda_N \tilde{\xi}_N \right\}.$$

Proof. The worst-case expected value $\sup_{\mathbb{P} \in \mathcal{D}} \mathbb{E}_{\mathbb{P}}[\mathcal{Q}(\mathbf{z}, \tilde{\xi})]$ can be written as

$$\begin{aligned} & \max_{\tilde{\xi} \in \Xi} \int \mathcal{Q}(\mathbf{z}, \tilde{\xi}) \, d\mathbb{P} \\ & \text{s.t. } \int_{\tilde{\xi} \in \Xi} \tilde{\xi}_E \, d\mathbb{P} = \mu_E, \quad \int_{\tilde{\xi} \in \Xi} \tilde{\xi}_N \, d\mathbb{P} = \mu_N, \quad \int_{\tilde{\xi} \in \Xi} d\mathbb{P} = 1. \end{aligned}$$

By taking the dual, we obtain

$$\begin{aligned} & \min \mu_E \lambda_E + \mu_N \lambda_N + \eta \\ & \text{s.t. } \lambda_E \tilde{\xi}_E + \lambda_N \tilde{\xi}_N + \eta \geq \mathcal{Q}(\mathbf{z}, \tilde{\xi}), \quad \forall \tilde{\xi} \in \Xi. \end{aligned}$$

where λ_E , λ_N , and η are dual variables. At optimality, we have $\eta^* = \max_{\tilde{\xi} \in \Xi} \{\mathcal{Q}(\mathbf{z}, \tilde{\xi}) - \lambda_E \tilde{\xi}_E - \lambda_N \tilde{\xi}_N\}$, which leads to the proposed formulation. \square

Proposition III.2. Given solution $(\mathbf{z}, \lambda_E, \lambda_N)$, the inner max-min problem can be reformulated as the following max problem:

$$\begin{aligned} \mathcal{Z}(\mathbf{z}, \lambda_E, \lambda_N, \tilde{\xi}) &= \max_{\tilde{\xi} \in \Xi} \mathbf{c}^T \mathbf{x} - \lambda_E \tilde{\xi}_E - \lambda_N \tilde{\xi}_N \quad (7a) \\ \text{s.t. } & 0 \leq \mathbf{A}\mathbf{x} + \mathbf{B}(\tilde{\xi})\mathbf{z} - \mathbf{d} \leq M(1 - \alpha), \\ & 0 \leq \beta \leq M\alpha, \quad \mathbf{A}^T \beta = \mathbf{c}, \quad \alpha \in \mathbb{B}^m. \end{aligned}$$

where M is a sufficiently large value.

Proof. Consider the following max-min problem:

$$\max_{\tilde{\xi} \in \Xi} \left(\min_{x \in \mathcal{X}(z, \tilde{\xi})} c^T x \right) - \lambda_E \tilde{\xi}_E - \lambda_N \tilde{\xi}_N$$

Using the complementary slackness condition, we obtain

$$\max_{\tilde{\xi} \in \Xi, x \in \mathbb{R}^n, \beta \in \mathbb{R}_+^m} c^T x - \lambda_E \tilde{\xi}_E - \lambda_N \tilde{\xi}_N \quad (9a)$$

$$\text{s.t. } Ax + B(\tilde{\xi})z \geq d, \quad A^T \beta = c, \quad (9b)$$

$$\beta^T (Ax + B(\tilde{\xi})z - d) = 0. \quad (9c)$$

where β is a dual vector, (9b) is primal and dual feasibility and (9c) is the complementary slackness. By introducing a big- M coefficient, constraints (9c) can be expressed as linear constraints, which leads to the formulation in (7). \square

A. Column-and-Constraint Generation (CCG) Algorithm

Using propositions (III.1) and (III.2), the two-stage DRO problem with a convex support-set is exactly solvable with the CCG algorithm [10]. Since the convex support set has infinitely many extreme points the CCG approach can be computationally intensive. To improve the computational performance of the CCG, we develop *two* tractable solution approaches that provide upper and lower bounds on the optimal value of problem (4).

Polyhedral support set

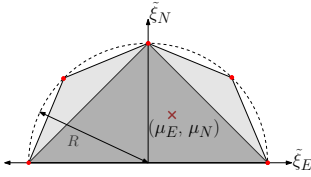


Fig. 4: Polyhedral support sets with 3 and 5 extreme points.

The first approach approximates the convex support set with a polytope that has N extreme points. When the polytope is a subset (resp. superset) of the support set (see Figure 4), it lower (resp. upper) bounds the optimal value of the original problem (4). In this section, we solve problem (4) with the polytope Ξ^N defined as $\text{conv}\{(\hat{\xi}_E^1, \hat{\xi}_N^1), \dots, (\hat{\xi}_E^N, \hat{\xi}_N^N)\}$. Since Ξ^N is also a convex set, strong duality (proposition III.1) holds. Thus, problem (4) with support set Ξ^N is also solvable using the CCG algorithm (algorithm (1)). Note that the CCG algorithm is guaranteed to converge in a finite number of iterations since the number of extreme points of Ξ^N is finite.

The CCG algorithm is a cutting plane method. The algorithm iteratively refines the feasible domain of the two-stage DRO problem by sequentially generating a set of recourse variables and their associated constraints. In algorithm (1), LB and UB denote the incumbent lower and upper bounds of problem (4), respectively. Step-2 evaluates the lower bound for problem (4) by solving the relaxed master problem. Step-3 finds the worst-case value of $\tilde{\xi}^*$ by enumerating all N extreme points and picks an optimal value. Step-4 updates the upper bound for the worst-case value of $\tilde{\xi}^*$. Steps 5-7 terminate the algorithm if the optimality gap is within a specified ϵ , else

Algorithm 1 CCG for 2-stage DRO with polyhedral support set

- 1: Set LB= $-\infty$, UB= ∞ , $t = 0$ and $\mathcal{T} = \emptyset$.
- 2: Update LB by solving the following master problem:

$$\text{LB} = \min_{z \in \mathcal{F}} q^T z + \mu_E \lambda_E + \mu_N \lambda_N + \eta \quad (10a)$$

$$\text{s.t. } \eta \geq c^T x^\ell - \lambda_E \xi_E^\ell - \lambda_N \xi_N^\ell, \quad \forall \ell \in \mathcal{T}, \quad (10b)$$

$$Ax^\ell + B(\tilde{\xi}^\ell)z \geq d, \quad \forall \ell \in \mathcal{T}. \quad (10c)$$

– Record an optimal solution z^* , λ_E^* , λ_N^* , and η^* .

- 3: Solve the following problem:

$$\max_{\tilde{\xi} \in \Xi^N} \left\{ Q(z^*, \tilde{\xi}) - \lambda_E^* \tilde{\xi}_E - \lambda_N^* \tilde{\xi}_N \right\}$$

– Record an optimal $\tilde{\xi}^*$ and the optimal value $Z(z^*, \lambda_E^*, \lambda_N^*, \tilde{\xi}^*)$

- 4: Update UB by

$$\text{UB} = \min\{\text{UB}, q^T z^* + \mu_E \lambda_E^* + \mu_N \lambda_N^* + Z(z^*, \lambda_E^*, \lambda_N^*, \tilde{\xi}^*)\}$$

- 5: **if** (UB – LB)/UB $\leq \epsilon$ **then**

6: Stop and return z^* as an optimal solution.

- 7: **else**

8: Update $\xi_E^{t+1} = \tilde{\xi}_E^*$, $\xi_N^{t+1} = \tilde{\xi}_N^*$, $\mathcal{T} = \mathcal{T} \cup \{t+1\}$ and $t = t+1$.

9: Go to step 2 and solve the updated master problem.

- 10: **end if**

steps 8-9 augment the master problem with the constraints and variables associated with extreme point $\tilde{\xi}^*$ and continues the iteration until an optimal solution for problem (4) is found.

B. Triangle support set: Exact tractable reformulation

As a special case, we further approximate the convex support set with a polytope that has *three* extreme points, i.e., Ξ^3 (see Figure 4). Once again, the CCG algorithm (algorithm (1)) can be used to solve model (4). However, with a triangle support set, we derive an exact monolithic reformulation as discussed below. This reformulation is solved efficiently using off-the-shelf commercial solvers such as CPLEX or Gurobi. In the numerical results section, we demonstrate the computational efficacy of this exact reformulation in detail.

Proposition III.3. For fixed $z \in \mathcal{F}$, the worst-case expected value $\sup_{p \in \mathcal{D}} \mathbb{E}_p[Q(z, \tilde{\xi})]$ with Ξ^3 is equivalent to

$$\max_{p \in \mathbb{R}_+^3} \sum_{k=1}^3 Q(z, \hat{\xi}^k) p_k \quad (11a)$$

$$\text{s.t. } \sum_{k=1}^3 \hat{\xi}_E^k p_k = \mu_E, \quad \sum_{k=1}^3 \hat{\xi}_N^k p_k = \mu_N, \quad \sum_{k=1}^3 p_k = 1. \quad (11b)$$

where $\{\hat{\xi}^1, \hat{\xi}^2, \hat{\xi}^3\}$ are the extreme points of the set Ξ^3 .

Proof. For fixed $z \in \mathcal{F}$, the function $Q(z, \tilde{\xi})$ is convex in $\tilde{\xi}$. Let \mathcal{H} be a convex hull of $\{(\tilde{\xi}, y) : \tilde{\xi} \in \Xi^3, y = Q(z, \tilde{\xi})\}$. Since taking expectation can be viewed as a convex combination, it follows that $(\mu, Q(z, \mu)) \in \mathcal{H}$. Since the set \mathcal{D} is a mean-support ambiguity set where the support set Ξ^3 is a simplex with 3 extreme points $\hat{\xi}^1, \hat{\xi}^2, \hat{\xi}^3$, there is a unique convex combination of the extreme points which yields μ . Therefore, we have $\sup_{p \in \mathcal{D}} \mathbb{E}_p[Q(z, \tilde{\xi})] = \sup\{y | (\mu, y) \in \mathcal{H}\}$, where μ is a convex combination of the 3 extreme points,

$\mu = \hat{\xi}^1 p_1 + \hat{\xi}^2 p_2 + \hat{\xi}^3 p_3$, and $y = Q(z, \hat{\xi}^1) p_1 + Q(z, \hat{\xi}^2) p_2 + Q(z, \hat{\xi}^3) p_3$. \square

Remark III.4. The optimal solution (p_1^*, p_2^*, p_3^*) to problem (11) is uniquely determined due to the unique convex combination of the extreme points which yields μ . In other words, we solve the following linear system of equations:

$$\begin{bmatrix} \hat{\xi}_E^1 & \hat{\xi}_E^2 & \hat{\xi}_E^3 \\ \hat{\xi}_N^1 & \hat{\xi}_N^2 & \hat{\xi}_N^3 \\ 1 & 1 & 1 \end{bmatrix} \begin{bmatrix} p_1 \\ p_2 \\ p_3 \end{bmatrix} = \begin{bmatrix} \mu_E \\ \mu_N \\ 1 \end{bmatrix}$$

As long as $\mu \in \Xi^3$, we have $p_1^*, p_2^*, p_3^* \geq 0$.

Proposition III.5. Problem (4) with triangle support set (Ξ^3) is equivalent to the following stochastic program:

$$\min_{z \in \mathcal{F}} q^T z + \sum_{k=1}^3 p_k^* (c^T x^k) \quad (12a)$$

$$s.t. Ax^k \geq d - B(\hat{\xi}^k)z, \forall k \in \{1, 2, 3\}. \quad (12b)$$

IV. NUMERICAL EXPERIMENTS

In this section, we conduct numerical experiments using the epri-21 system, which is specifically designed for GMD studies. Most parameters in our models can be obtained from [18]. The remaining parameters include $\kappa^l = 50,000[\$/p.u.]$, $\kappa^s = 100,000[\$/p.u.]$, $\bar{v}^d = 10,000 [V]$, and $\bar{I}_e^{\text{eff}} = 2 \frac{\bar{s}_e}{\min(\bar{v}_i, \bar{v}_j)} [\text{Amp}]$, $\forall e_{ij} \in \mathcal{E}^T$. For each system, we generate instances which vary the mean values (μ_E, μ_N) and the maximum magnitude R of the geo-electric field (all units are in [V/km]). Computations were performed with the HPC resources at Los Alamos National Laboratory with Intel Xeon CPU E5-2660v3, 2.60GHz and 120GB of memory. Optimization models were solved using Gurobi v8.1.0 and were implemented in C++.

A. The epri-21 system

Figure 5 shows a simplified diagram of the epri-21 system geo-located near Atlanta, GA. This system has 19 buses, 7 generators, 15 transmission lines, 16 transformers, and 8 substations. In the diagram, the blue lines are 500kV and the green lines are 345kV (see [18] for details).

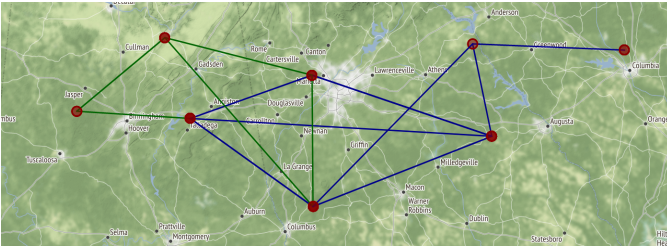


Fig. 5: The epri-21 system

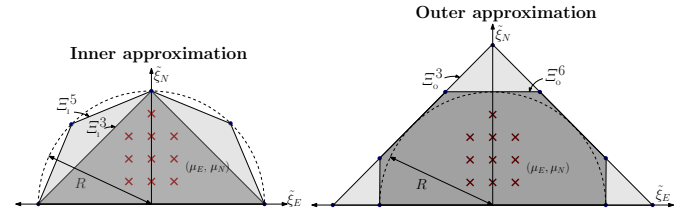


Fig. 6: Polyhedral support sets that inner- (left) and outer- (right) approximate the nonlinear uncertainty set Ξ .

B. Uncertainty data sets

We consider ten different instances that vary the mean values (μ_E, μ_N) in proportion to R (Table III). For each instance, we construct four different polyhedral support sets: (1) triangle (Ξ_1^3) and (2) pentagon (Ξ_1^5) that inner-approximates the convex support set and (3) triangle (Ξ_0^3) and (4) hexagon (Ξ_0^6) that outer-approximates the convex support set as depicted in Figure 6. The objective function values of prob. (4) with these sets are non-increasing in the order: $\Xi_0^3, \Xi_0^6, \Xi, \Xi_1^5$, and Ξ_1^3 .

Instance #	(μ_E, μ_N) [V/km]	Instance #	(μ_E, μ_N) [V/km]
1	(0, R/5)	6	(R/5, 2R/5)
2	(0, 2R/5)	7	(R/5, 3R/5)
3	(0, 3R/5)	8	(-R/5, R/5)
4	(0, 4R/5)	9	(-R/5, 2R/5)
5	(R/5, R/5)	10	(-R/5, 3R/5)

TABLE III: Ten different (μ_E, μ_N) depending on R values.

C. Quality of uncertainty set approximation

Since support set Ξ_1^3 has the lowest objective function value for the 4 polyhedral sets, we normalize all the objective function values with respect to that of Ξ_1^3 . Figure 7 shows the normalized objective function values of the DRO model for the 4 polyhedral sets on the 10 instances that have $R = 5$ (left) and $R = 15$ (right). With support sets Ξ_1^3 and Ξ_0^3 , the optimality gaps are less than 0.02% and 0.49% for $R = 5$ and $R = 15$, respectively. With support sets Ξ_1^5 and Ξ_0^6 , the optimality gaps are reduced to 0.01% and 0.03% when $R = 5$ and $R = 15$, respectively. Based on these optimality gaps for the epri-21 system, we observe that the triangle support set is a very good approximation of the convex support set.

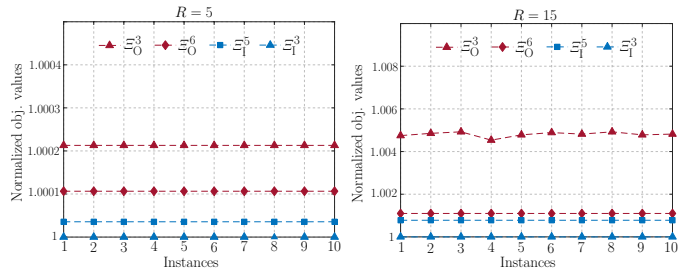


Fig. 7: Normalized objective function values for $R = 5, 15$.

D. Computational performances

In this section, for $R \in \{5, 7.5, 10, 12.5, 15\}$, we construct 10 instances with mean values described in Table III. Figure

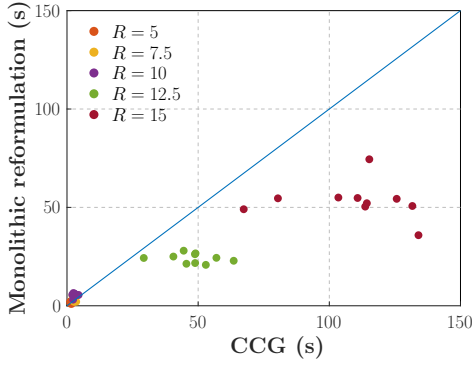


Fig. 8: Computational times (sec.) of monolithic reformulation and CCG algorithm with the triangle support set (Ξ_1^3).

8 compares the exact monolithic reformulation (section III-B) with the CCG algorithm (algorithm 1) using the Ξ_1^3 formulation. All the points located below the 45 degree blue line are instances where the monolithic reformulation computationally outperforms the CCG algorithm. For larger uncertainty sets ($R = 15$), the monolithic reformulation is on an average 2.1 times faster than CCG. The tightness of the triangle-set approximation (see section IV-C) and the computational efficacy of the exact reformulation provides evidence that the monolithic approach is very effective at solving the DRO.

E. Planning mitigation solutions for uncertain GMDs

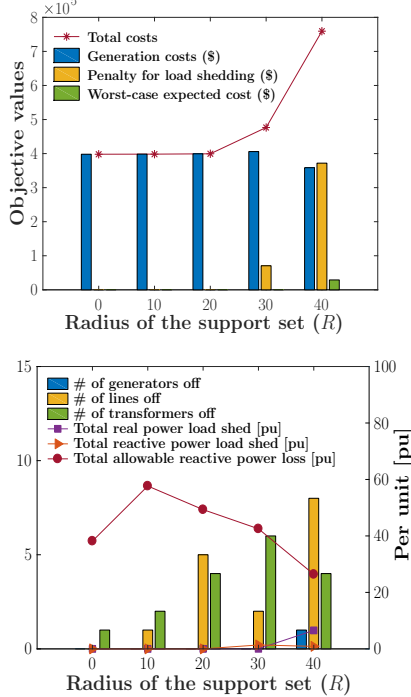


Fig. 9: Optimal objectives and solutions for various R values.

In this section, we consider how the solutions change when the mean and magnitude of the GMD are varied. Here, the mean values are $(\mu_E, \mu_N) = (5, 4)$ and $R \in \{0, 10, 20, 30, 40\}$.

$R = 0$ indicates a deterministic model with $(\tilde{\xi}_E, \tilde{\xi}_N) = (\mu_E, \mu_N) = (5, 4)$.

In Figure 9, the optimal objective values (top) and mitigation actions (bottom) change as the size of the uncertainty set (R) increases. As expected, as R increases, more generators, lines, and transformers are turned off to mitigate the effect of GMDs and address a larger number of worst-case scenarios. The negative impacts of GMDs can be mitigated without shedding loads (only using line and transformer switching) for $R \leq 20$. However, when $R \geq 10$, the total allowable reactive power losses (2)'s solution, bottom figure) decreases, indicating that the topological control actions can mitigate these losses, thus potentially reducing the need for expensive blocking devices used in the network. When $R \geq 30$, the topological control actions are not sufficient to handle the uncertainty in the GMD and some real and reactive power loads are shed. This is reflected in the increase in the total cost of the objective value at $R = 40$.

V. CONCLUSIONS

In this paper, we developed a novel two-stage DRO model which uses control of transmission lines, generators, and transformers to mitigate potential negative impacts of uncertain GMDs. This model minimizes the expected total cost of mitigation for the worst-case distribution in a convex support set of the GMD's uncertainty and subject to convex relaxations of the AC power flow and GMD constraints. Given this convex support set and mean values for the uncertain GMDs, our DRO model is solvable using the CCG algorithm. However, there are no guarantees of finite time convergence. Instead, we approximated the support set with a polytope with N extreme points that allows the CCG to terminate with a finite number of iterations ($O(N)$). We further reformulated the two-stage DRO model into a monolithic MISOCP for the special case when the support set contains three extreme points. We numerically showed the run-time efficacy of this reformulation. Finally, we provided a detailed case study on epri-21 system which analyzed the effects of modeling uncertain GMDs.

There are a number of interesting future directions for this work. *First*, given the tightness of the triangle support set approximation and the computational efficacy of the exact reformulation, this approach could be used to warm-start the CCG algorithm and speed up the convergence in cases with N extreme points. *Second*, the approximation could be tightened further by considering different choices of the extreme points for the triangle. *Third*, the corrective actions obtained in this paper may not necessarily be feasible to the original nonconvex AC power flow and GMD constraints. Thus AC feasible solution recovery will be important from the practical perspective, albeit this may be non-trivial for the DRO version of the problem. *Finally*, it will be important to scale the DRO to cases with 100's or even 1000's of nodes.

Acknowledgements This work was supported by the U.S. Department of Energy LDRD program at Los Alamos National Laboratory under "Impacts of Extreme Space Weather

REFERENCES

- [1] United States Government Accountability Office, "Critical infrastructure protection: Protecting the electric grid from geomagnetic disturbances," Dec 2018. [Online]. Available: www.gao.gov/assets/700/696140.pdf
- [2] D. Boteler, R. Pirjola, and H. Nevanlinna, "The effects of geomagnetic disturbances on electrical systems at the earth's surface," *Advances in Space Research*, vol. 22, no. 1, pp. 17–27, 1998.
- [3] J. Gannon, A. Swidinsky, and Z. Xu, *Geomagnetically Induced Currents from the Sun to the Power Grid*. John Wiley & Sons, 2019, vol. 246.
- [4] L. Bolduc, "GIC observations and studies in the hydro-québec power system," *Journal of Atmospheric and Solar-Terrestrial Physics*, vol. 64, no. 16, pp. 1793–1802, 2002.
- [5] L. Bolduc, M. Granger, G. Pare, J. Saintonge, and L. Brophy, "Development of a DC current-blocking device for transformer neutrals," *IEEE Transactions on power delivery*, vol. 20, no. 1, pp. 163–168, 2005.
- [6] H. Zhu and T. J. Overbye, "Blocking device placement for mitigating the effects of geomagnetically induced currents," *IEEE Trans. on Power Systems*, vol. 30, no. 4, pp. 2081–2089, 2014.
- [7] M. Lu, H. Nagarajan, E. Yamangil, R. Bent, S. Backhaus, and A. Barnes, "Optimal transmission line switching under geomagnetic disturbances," *IEEE Trans. on Power Systems*, vol. 33, no. 3, pp. 2539–2550, 2017.
- [8] M. Kazerooni and T. J. Overbye, "Transformer protection in large-scale power systems during geomagnetic disturbances using line switching," *IEEE Trans. on Power Systems*, vol. 33, no. 6, pp. 5990–5999, 2018.
- [9] M. Lu, S. D. Eksioglu, S. J. Mason, R. Bent, and H. Nagarajan, "Distributionally robust optimization for a resilient transmission grid during geomagnetic disturbances," *arXiv preprint:1906.04139*, 2019.
- [10] B. Zeng and L. Zhao, "Solving two-stage robust optimization problems using a column-and-constraint generation method," *Operations Research Letters*, vol. 41, no. 5, pp. 457–461, 2013.
- [11] J. R. Woodroffe, S. Morley, V. Jordanova, M. Henderson, M. Cowee, and J. Gjerloev, "The latitudinal variation of geoelectromagnetic disturbances during large ($\text{dst} \leq -100$ nt) geomagnetic storms," *Space Weather*, vol. 14, no. 9, pp. 668–681, 2016.
- [12] B. Kocuk, S. S. Dey, and X. A. Sun, "New formulation and strong MISOCP relaxations for AC optimal transmission switching problem," *IEEE Trans. on Power Systems*, vol. 32, no. 6, pp. 4161–4170, 2017.
- [13] M. Lu, H. Nagarajan, R. Bent, S. D. Eksioglu, and S. J. Mason, "Tight piecewise convex relaxations for global optimization of optimal power flow," in *Power Systems Computation Conference (PSCC)*. IEEE, 2018, pp. 1–7.
- [14] M. R. Narimani, D. K. Molzahn, H. Nagarajan, and M. L. Crow, "Comparison of various trilinear monomial envelopes for convex relaxations of optimal power flow problems," in *IEEE Global Conference on Signal and Information Processing (GlobalSIP)*. IEEE, 2018, pp. 865–869.
- [15] H. Nagarajan, E. Yamangil, R. Bent, P. Van Hentenryck, and S. Backhaus, "Optimal resilient transmission grid design," in *2016 Power Systems Computation Conference (PSCC)*. IEEE, 2016, pp. 1–7.
- [16] D. K. Molzahn, I. A. Hiskens *et al.*, *A survey of relaxations and approximations of the power flow equations*. Now Publishers, 2019.
- [17] H. Nagarajan, M. Lu, E. Yamangil, and R. Bent, "Tightening McCormick relaxations for nonlinear programs via dynamic multivariate partitioning," in *International Conference on Principles and Practice of Constraint Programming*. Springer, 2016, pp. 369–387.
- [18] R. Horton, D. Boteler, T. J. Overbye, R. Pirjola, and R. C. Dugan, "A test case for the calculation of geomagnetically induced currents," *IEEE Transactions on Power Delivery*, vol. 27, no. 4, pp. 2368–2373, 2012.